Biophysical Journal, Volume *113*

Supplemental Information

Allosteric Modulation of Intact γ-Secretase Structural Dynamics

Ji Young Lee, Zhiwei Feng, Xiang-Qun Xie, and Ivet Bahar

Supplemental Methods

Analysis of Collective Modes using the Elastic Network Models ANM

In the ANM, the protein is represented as a network where residues serve as the nodes, the positions of which are identified by those of α-carbons, and the overall potential is represented as the sum of harmonic potentials between interacting nodes (C^{α}-C^{α} < 15Å) (1). The force constants for the *3N* × *3N* interactions (for *N* residues in *3D*) are given by the elements of the Hessian matrix **H**. The inverse $\mathbf{H}^{-1}$ is proportional to the covariance of residue fluctuations away from their mean position. To achieve a conformation displaced along one of the ANM modes, we use the following equation: $\mathbf{R}^{(k)} = \mathbf{R}^{(0)} \pm s\lambda_k^{-1/2} \boldsymbol{u}_k$, where $\mathbf{R}^0$ is a *3N*-dimensional vector representing initial coordinates, λ_k is eigenvalue, and $\boldsymbol{u}_k$ is corresponding eigenvectors. We choose *s* where ANM conformers deviates by an RMSD of 4 Å from the initial structure (in **Figs. 2, 5, 8, S4, and S6**).

We used structure of γ-secretase (PDB ID 5FN2) (2) which has total 1309 residues and built membrane using an FCC lattice with a distance of 6.2 Å between nearest neighbors with 7 layers and a circular shape with 80 Å radius from the center of the protein (total 3108 nodes for membrane). The protein was positioned into membrane using Orientations of Proteins in Membrane (OPM) database (3). Our system has total 4417 nodes (*N*=4417) and *3N-6* (13245) modes form a complete basis set for all possible motions of the *3N*-dimensional structure. The ANM calculation of γ-secretase in the absence of membrane in **Fig. 1D** uses only protein structure (N=1309). All computations were performed using the ProDy API (4,5).

PULCHRA version 3.04 program (6) was used to add all backbone and side chain atoms to the conformers generated by the ANM. Energy-minimization was performed using NAMD for 2,000 steps.

Coarse-grained Molecular Dynamics Simulations

The coarse-grained system of γ-secretase (PDB ID 5FN2) (2) and lipid bilayer and MD set-up was prepared using GHARMM-GUI Martini bilayer maker (7), and simulations were performed using GROMACS version 5.1.4 (8) with MARTINI force field v2.2 (9). All the systems were relaxed using equilibration steps, and two independent NPT simulations were performed for 10 μs each with 20 fs time step. The temperature was set to 310 K using V-rescale coupling, and the pressure was set to 1.0 bar using semi-isotropic Parrinello-Rahman coupling. The system has 1,309 residues, 414 POPC lipid sites, 13,355 water molecules, 155 Na^+ ions, and 150 Cl^- ions, i.e. a total of 21,561CG sites simulated in a 130 Å x 130 Å x 150 Å box.

Principal Component Analysis (PCA) of MD Trajectories

The principal component analysis using MD snapshots or experimental structures was used to extract principal changes in structure (4,10). Principal modes were obtained by decomposing the covariance matrix **C** for each dataset as $\mathbf{C} = \sum_{i=1}^{3N} \sigma_i \boldsymbol{P}^{(i)} \boldsymbol{P}^{(i)T}$ where $\boldsymbol{P}^{(i)}$ and σ_i are the respective *i*th eigenvalue and eigenvector of **C**, σ_i corresponding to the largest variance component. The fractional contribution of the principal component (eigenvector) $\boldsymbol{P}^{(i)}$ to structural variance in the dataset is given by $f_i = \sigma_i / \sum_j \sigma_j$ where the summation is preformed over all components (note that σ_i is equivalent to $1/\lambda_i$ obtained from ANM). All computations were performed using the ProDy API (4,5).

Druggability Simulations and Trajectory Analysis

All atom MD systems and set-up were prepared using DruGUI (11) in VMD (12). We performed 3 independent simulations of intact γ-secretase (PDB ID 5FN2) including probe molecules in a water box. Our system has 25,600 water and 1,280 probe molecules, which gives a ratio of 20 water molecules per probe molecule as used in our previous study (11). The probe molecules were evenly distributed in the box. We included four different probe molecules, 896 isopropanol (70%), 128 isopropylamine (10%), 128 acetate (10%), and 128 acetamide (10%) molecules. The system contained a total of 112,132 atoms of protein, probes, waters, and ions. MD simulations were performed using NAMD (13), and we relaxed the systems using equilibration steps and performed NPT dynamics for 40 ns for each (total 120 ns) with 2 fs time step. Nosé-Hoover constant pressure (1 bar) and temperature (300 K) were used. We also performed 5 independent all atom MD simulations including probe molecules for the PS1 subunit of γ-secretase (PDB ID 5FN2). This system includes 252 isopropanol (70%), 36 isopropylamine (10%), 36 acetate (10%), 36 acetamide (10%), and 7200 water molecules. Other simulation setups are same as in intact protein.

For trajectory analysis, all MD snapshots were superposed onto the reference PDB structure of the protein using C^{α} atoms and a cubical grid-based representation of the space. Grid edge size was set to 0.5 Å. Probe molecules having a nonhydrogen atom within 2.5 Å from protein atoms were considered to interact with the protein. For each probe type, the individual occupancy of grids was calculated using their central carbon atoms. We obtain occupancy of each probe for a given voxel. High occupancy voxels, called hot spots, within a distance less than 5.5 Å were merged and druggable sites were defined upon merger of at least 6 hot spots. More details are available in our previous study (11) as well as ProDy tutorial. All computations were performed using DruGUI in the ProDy API (4,5).

Docking of Small Molecules

The PDB structure of γ-secretase (2) was used as target for docking γ-secretase ligands, including DAPT, BMS-708163, CHEMBL2159511, CHEMBL2159687 and CHEMBL2159691, and γ-

secretase modulators of E2012 and ST1120. Also, the closed ANM conformers along mode 1 (**Fig. 5**), mode 7 (**Fig. S4**), and mode 14, and the open conformer along ANM mode 14 (**Fig. 8**) were used as targets. Surflex-Dock, a docking program implemented in SYBYL-X 1.3, was used to generate detailed receptor-ligands interactions. We used the same protocol for docking as reported in our previous publications (14-17). Briefly, (**A**) energy minimizations of 3D structure of γ-secretase was performed using SYBYL-X 1.3. The parameters defined in the SYBYL were as follows: Gradient was set to 0.5 kcal/mol, max iterations were set to 5000, force field was selected as MMFF94s, and that for the charges was MMFF94. (**B**) The putative binding cavity of γ-secretase was predicted and generated using SYBYL-X 1.3 by a similar protocol, with the Threshold set to 0.50 while the Bloat was set to 0. (**C**) The following docking parameters were used. (a) The number of starting conformations per ligand was set to 10; max conformations per fragment was set to 20, (b) maximum number of rotatable bonds per molecule was 100, (c) the flags were turned on at pre-dock minimization, post-dock minimization, molecule fragmentation, soft grid treatment, (d) activate spin alignment method with density of search was set to 9.0, and (e) number of spins per alignment was set to 12. (**D**) Result optimizations were carried out by allowing the protein movements with both hydrogen and heavy atoms.

REFERENCES

1. Atilgan, A. R., S. R. Durell, R. L. Jernigan, M. C. Demirel, O. Keskin, and I. Bahar. 2001. Anisotropy of fluctuation dynamics of proteins with an elastic network model. *Biophys. J.* 80:505-515.

2. Bai, X. C., E. Rajendra, G. H. Yang, Y. G. Shi, and S. H. W. Scheres. 2015. Sampling the conformational space of the catalytic subunit of human γ-secretase. *Elife* 4.

3. Lomize, M. A., A. L. Lomize, I. D. Pogozheva, and H. I. Mosberg. 2006. OPM: orientations of proteins in membranes database. *Bioinformatics* 22:623-625.

4. Bakan, A., L. M. Meireles, and I. Bahar. 2011. ProDy: protein dynamics inferred from theory and experiments. *Bioinformatics* 27:1575-1577.

5. Bakan, A., A. Dutta, W. Mao, Y. Liu, C. Chennubhotla, T. R. Lezon, and I. Bahar. 2014. Evol and ProDy for bridging protein sequence evolution and structural dynamics. *Bioinformatics* 30:2681-2683.

6. Rotkiewicz, P. and J. Skolnick. 2008. Fast procedure for reconstruction of full-atom protein models from reduced representations. *J. Comput Chem.* 29:1460-1465.

7. Qi, Y., H. I. Ingolfsson, X. Cheng, J. Lee, S. J. Marrink, and W. Im. 2015. CHARMM-GUI Martini maker for coarse-grained simulations with the Martini force field. *J. Chem. Theory Comput* 11:4486-4494.

8. Szilárd Páll, Mark James Abraham, Carsten Kutzner, Berk Hess, and Erik Lindahl. 2015. Tackling exascale software challenges in molecular dynamics simulations with GROMACS. *Solving Software Challenges for Exascale* 8759:3-27.

9. de Jong, D. H., G. Singh, W. F. Bennett, C. Arnarez, T. A. Wassenaar, L. V. Schafer, X. Periole, D. P. Tieleman, and S. J. Marrink. 2013. Improved parameters for the Martini coarse-grained protein force field. *J. Chem. Theory Comput* 9:687-697.

10. Amadei, A., A. B. Linssen, and H. J. Berendsen. 1993. Essential dynamics of proteins. *Proteins* 17:412-425.

11. Bakan, A., N. Nevins, A. S. Lakdawala, and I. Bahar. 2012. Druggability assessment of allosteric proteins by dynamics simulations in the presence of probe molecules. *Journal of Chemical Theory and Computation* 8:2435-2447.

12. Humphrey, W., A. Dalke, and K. Schulten. 1996. VMD: visual molecular dynamics. *J. Mol. Graph.* 14:33-38.

13. Phillips, J. C., R. Braun, W. Wang, J. Gumbart, E. Tajkhorshid, E. Villa, C. Chipot, R. D. Skeel, L. Kale, and K. Schulten. 2005. Scalable molecular dynamics with NAMD. *J. Comput Chem.* 26:1781-1802.

14. Feng, Z., M. H. Alqarni, P. Yang, Q. Tong, A. Chowdhury, L. Wang, and X. Q. Xie. 2014. Modeling, molecular dynamics simulation, and mutation validation for structure of cannabinoid receptor 2 based on known crystal structures of GPCRs. *J. Chem. Inf. Model.* 54:2483-2499.

15. Feng, Z., L. V. Pearce, X. Xu, X. Yang, P. Yang, P. M. Blumberg, and X. Q. Xie. 2015. Structural insight into tetrameric hTRPV1 from homology modeling, molecular docking, molecular dynamics simulation, virtual screening, and bioassay validations. *J. Chem. Inf. Model.* 55:572-588.

16. Xie, X. Q., J. Z. Chen, and E. M. Billings. 2003. 3D structural model of the G-protein-coupled cannabinoid CB2 receptor. *Proteins* 53:307-319.

17. Chen, J. Z., J. Wang, and X. Q. Xie. 2007. GPCR structure-based virtual screening approach for CB2 antagonist search. *J. Chem. Inf. Model.* 47:1626-1637.

Supplemental Figures

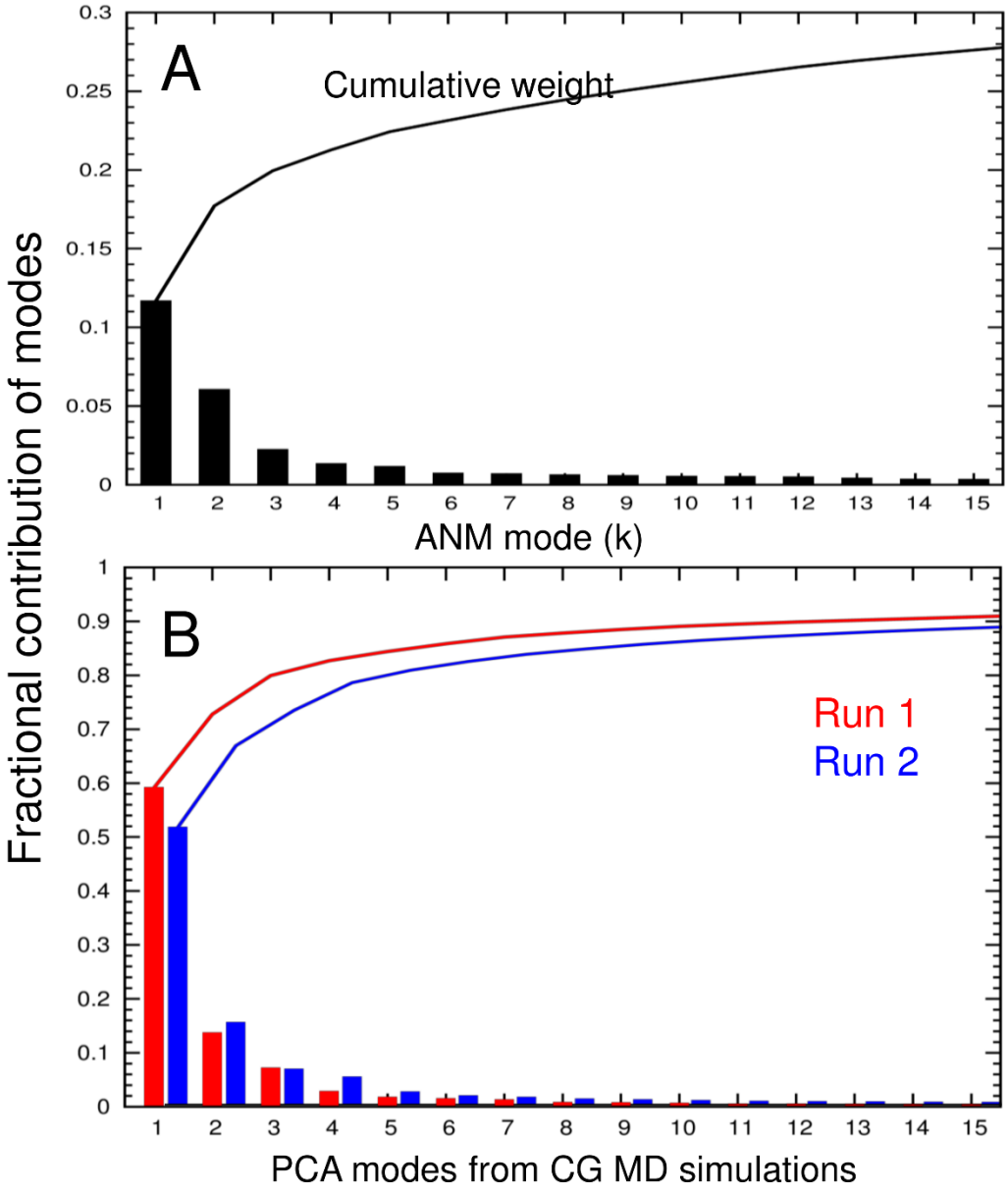

Figure S1. Eigenvalue spectrum obtained by ANM analysis and PCA of two CG MD trajectories generated for γ-secretase complex. (A) Inverse eigenvalues plotted against ANM mode index. The bar values are $(1/\lambda_k) / \Sigma(1/\lambda_k)$, where *k* is mode number, λ_k is eigenvalue of mode *k*, and Σ is summation over all modes (total of 3N-6 modes, N is 1309, γ-secretase residue numbers, using the system-environment method in ProDy). The cumulative contribution summed over all modes is shown. **(B)** Same distribution obtained from PCA of the covariance generated from CG MD runs 1 and 2.

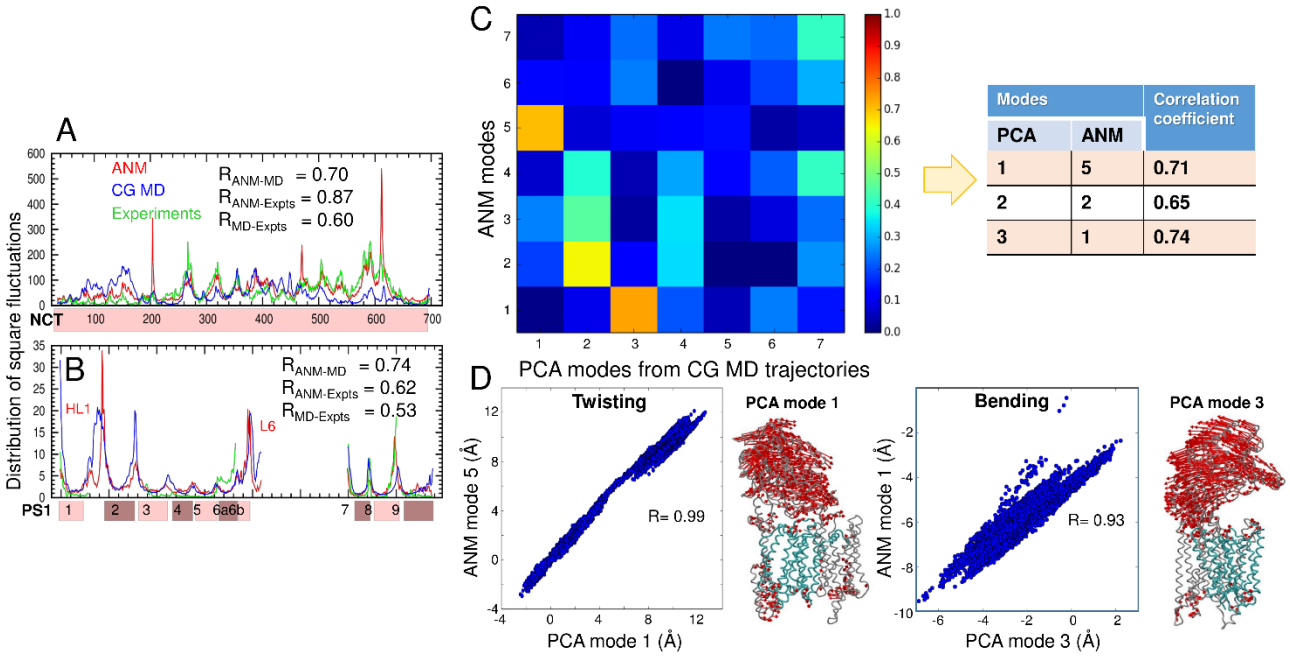

Figure S2. Mobility of γ-secretase observed in CG MD simulations. The panels represent the same properties, as in **Fig. 3**, but we displayed here the results from the 2nd CG MD run.

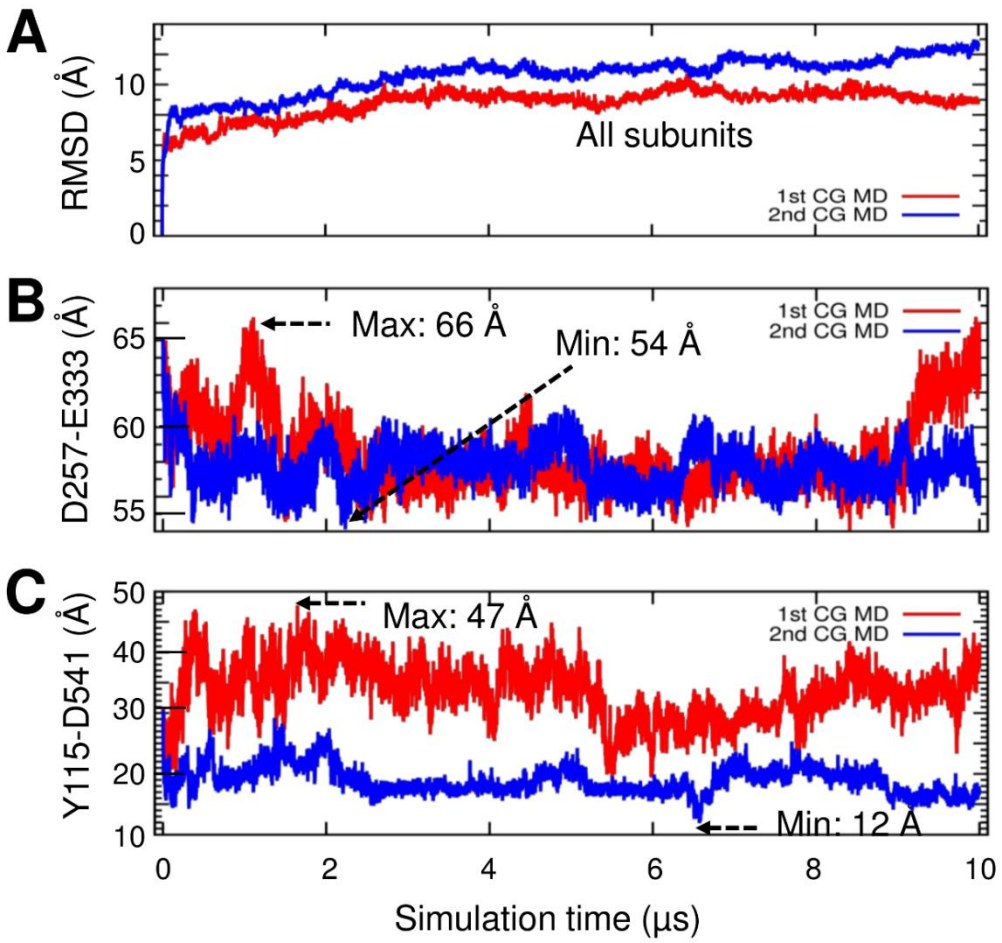

Figure S3. Mobility of NCT with respect to PS1 in CG MD simulations. (A) RMSD of whole protein including the four subunits for two independent 10 μs simulations. 1st and 2nd simulations are in *red* and *blue lines*, respectively. **(B)** Time evolution of the distance between D257(PS1) and E333(NCT). **(C)** Time evolution of the distance between Y115(PS1) and D541(NCT). Maximum and minimum distances are indicated by arrows in both panels **(B)** and **(C)**.

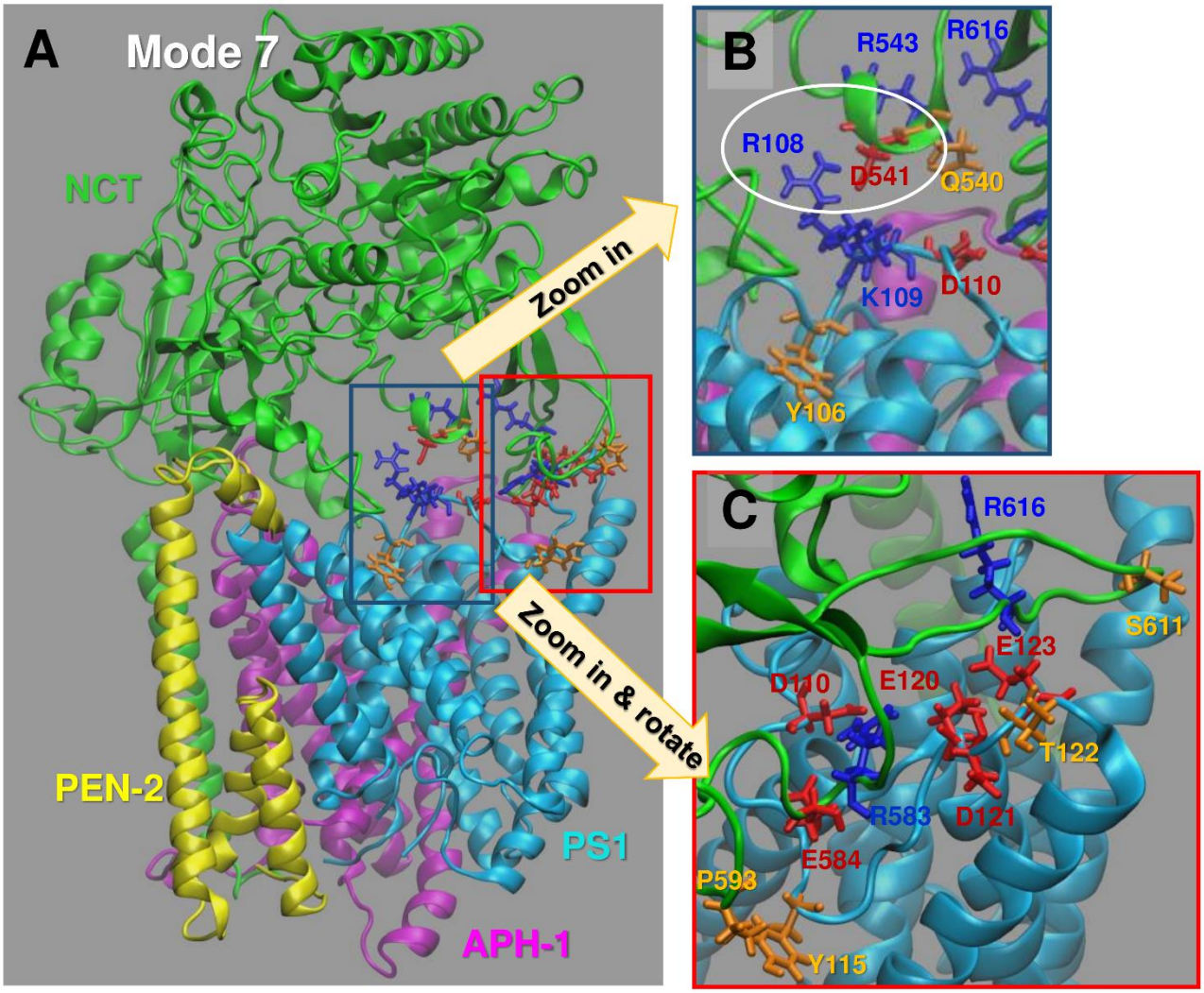

Figure S4. NCT and PS1 residues distinguished by their high mobility make intersubunit contacts facilitated by the global bending mode of the complex. **(A)** Closed form attainable upon reconfiguration of the complex along ANM mode 7. The size of the motion along mode 7 has been selected to yield an RMSD of 4 Å from the initial structure. Residues Q540, D541, R543, R583, E584, P593, S611, and R616 in NCT, and Y106, R108, K109, D110, Y115, E120, D121, T122, and E123 in the hydrophilic loop HL1 of PS1 are shown in *sticks* colored *red* (negatively charged), *blue* (positively charged), or *orange* (polar). We note the inter-subunit salt bridge D541-R108 (encircled in **B**). See also **Fig. 2** and **Table S1** for inter-residue and inter-atomic distances in the closed form.

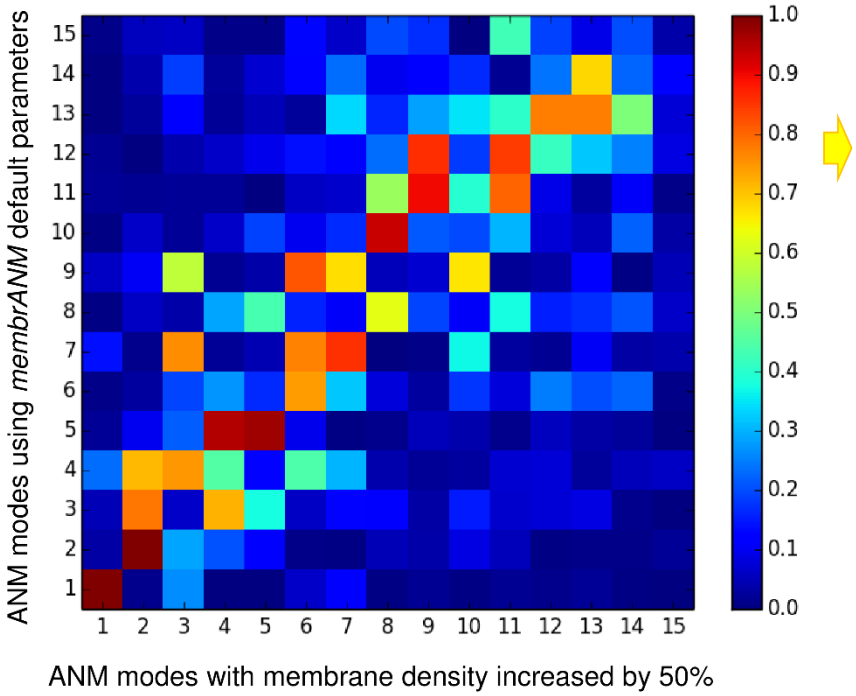

ANM Modes		R
membrane density		
default	high	
1	1	1.00
2	2	1.00
5	5	0.97
7	7	0.86
10	8	0.94
11	9	0.90
12	11	0.84

Figure S5. Comparison of the soft modes obtained for γ-secretase-membrane system using two different densities for the lipid bilayer. The ordinate refers to the original membrANM modes, obtained with default parameters in ProDy. The abscissa are the results obtaining by building a denser network model for the membrane (using 50% more network nodes). The diagram shows the correlation between the two sets of ANM modes, after taking the absolute values of the eigenvectors (as both directions of fluctuations are equivalent). The table on the right lists the correlation coefficients between selected pairs, the high density referring to the abscissa of the correlation map.

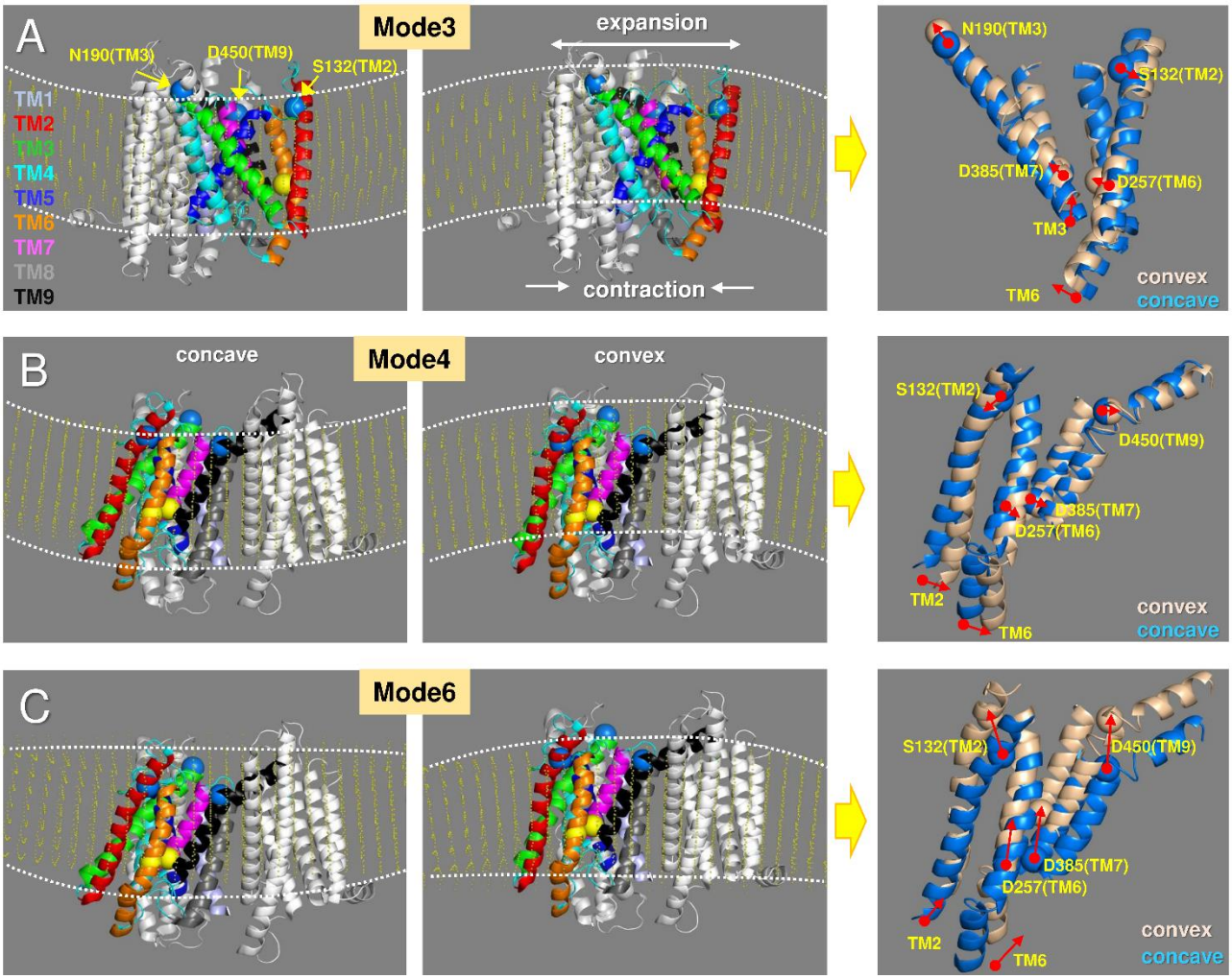

Figure S6. Motions of PS1 predicted by *membrANM* analysis of the intact protein. (A-C) Pair of conformers sampled during the motion of ANM modes 3, 4, and 6. Two ANM conformers which deviate by a preset RMSD of 4 Å from the initial structure are shown in each case. Modes 4 and 6 are shown from the same perspective; mode 3 is shown form a different perspective. We display APH-1 and PEN-2 in *silver*, the membrane in *yellow*, the PS1 TMs in different colors (NCT is not shown here). D257 and D385 in PS1 are shown in *yellow* spheres, S132 (TM2), N190 (TM3), and D450 (TM9) in *blue* spheres. On the *right* panels in each row, we display the superposition of the two conformers in different colors. For clarity, we included four TMs (TM2, TM3, TM6, and TM7 in mode 3 and TM2, TM6, TM7, and TM9 in modes 4 and 6). *Red arrows* indicate movements from concave to convex states for selected residues or TM helices. ANM mode 4 induces an opening at the EC-facing region but it is along an orthogonal radial direction such that it results in a change in TM2-TM9 distance. ANM mode 6 induces a vertical movement, in contrast to the previous two modes that induce radial displacements. We observe displacements in TM2, TM6 and TM9.

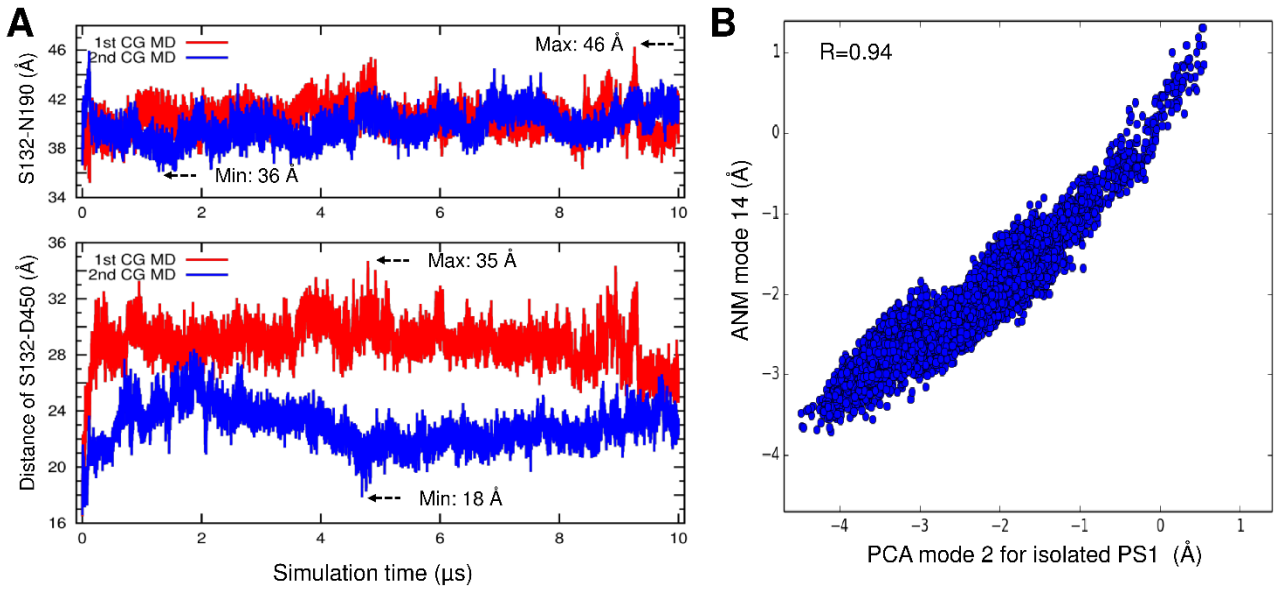

Figure S7. Mobility of PS1 in CG MD simulations. (A) Distances of the S132-N190 (*upper panel*) and S132-D450 (*lower panel*) are shown for two independent 10 μs simulations. The distances of 1st and 2nd simulations are in *red* and *blue lines*, respectively. From the two simulations, the maximum and minimum distances were indicated with *arrows*. **(B)** Projections of the 10,000 frames from the 2nd 10 μs trajectory onto the ANM mode 14 and PCA mode 2 directions.

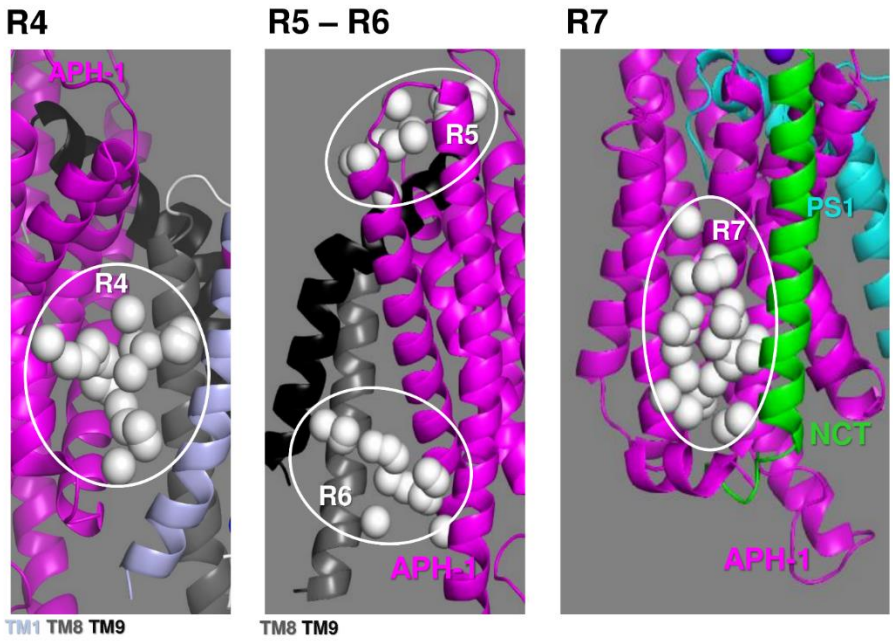

Figure S8. Druggable sites identified at APH-1 interfacial regions. Druggable regions R4-R7 were deduced from druggability simulations performed for the intact protein. White spheres are druggable hot spots, circled and labeled as R4-R7. R4-R6 are at the interface between PS1 and APH-1 (APH-1 is shown in *magenta* and TM helices in PS1 are colored as in **Fig. 9**. R7 is at the interface between APH-1 and NCT TM helix (*green*). Each panel shows the close vicinity of the druggable sites.

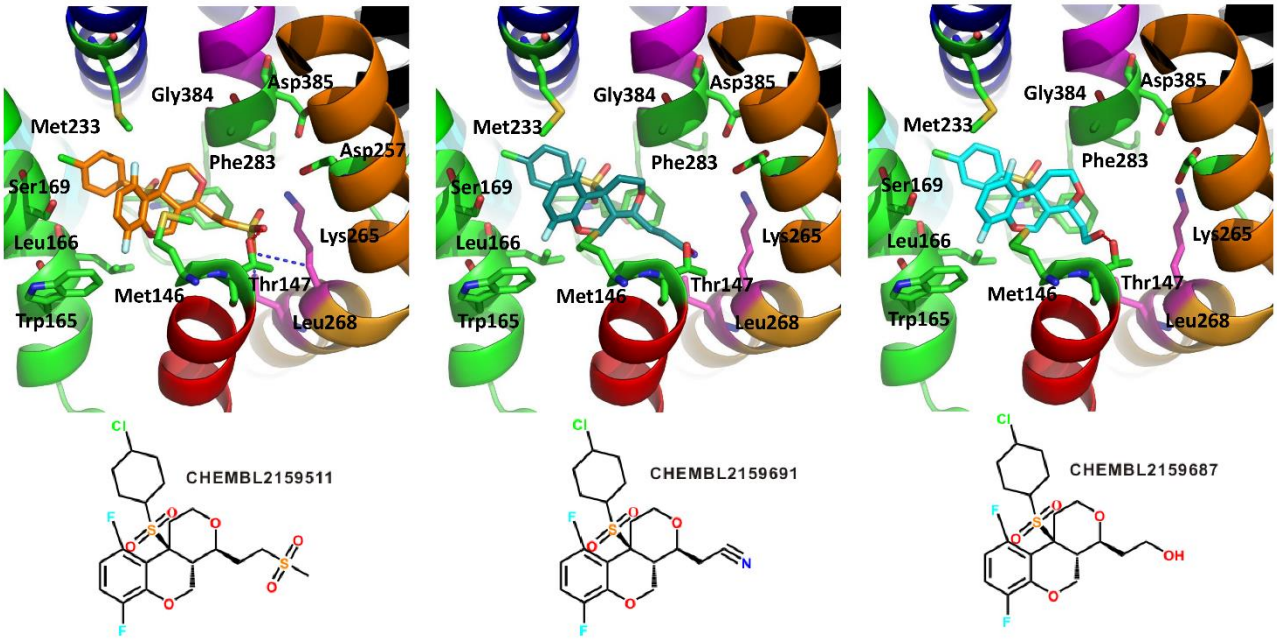

Figure S9. Detailed interactions between PS1 and three other drugs. Trp165, Leu166 and Met233 interact with the fluorine on the aromatic ring. Hydrophobic interactions take place between the Met146 and Phe283. Thr147 forms a hydrogen bond with (methylsulfonyl)ethane, acetonitrile, and ethanol, respectively.

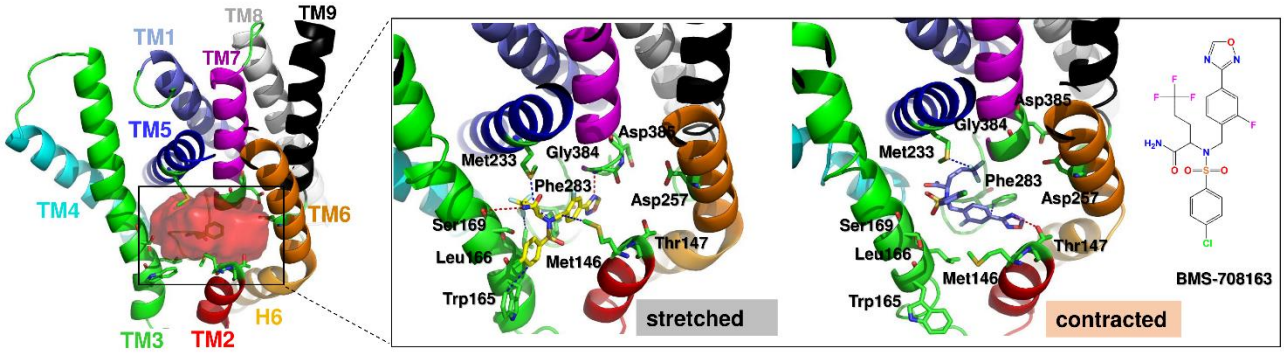

Figure S10. Dependency of the interactions between PS1 and its inhibitor (BMS-708163) on structural changes driven by ANM mode 4. The inhibitor binds to the orthosteric site (site R1 in **Fig. 9A**). Binding poses to the stretched and contracted forms are shown. The inhibitor shows a higher affinity to bind the stretched conformer.

Supplemental Tables

Table S1. Intersubunit distances between NCT and PS1 HL1 residue pairs that undergo intersubunit contacts facilitated by the global bending mode of the complex (*)

A

Mode 1: C^{α}-C^{α} distances (Å) between NCT and PS1 (closed state distances < 9 Å)

NCT	PS1	closed	open (PDB)
ASP541	**THR122**	**3.908**	**15.077**
ASP541	**ASP121**	**5.257**	**16.886**
GLN540	**THR122**	**5.350**	**16.531**
ARG543	**THR122**	**6.861**	**18.243**
ASP541	GLU123	6.880	17.275
LEU542	THR122	7.073	18.154
SER544	THR122	7.283	17.290
GLN540	ASP121	7.565	18.775
SER544	GLU123	8.125	18.534
GLN540	GLU123	8.324	18.860
ASP541	GLU120	8.369	18.871
ARG539	THR122	8.697	19.720
ARG543	GLU123	8.901	19.927
GLN540	THR124	8.970	20.558

B

Atomic interactions closer than 4 Å

ASP541	CA	THR122	OG1	3.825
ASP541	N	THR122	OG1	3.631
ASP541	CA	ASP121	C	3.973
ASP541	CA	ASP121	O	3.643
ASP541	CB	ASP121	O	3.716
ASP541	O	ASP121	O	3.579
GLN540	CA	THR122	OG1	3.969
GLN540	CB	THR122	OG1	3.948
GLN540	CD	THR122	OG1	3.196
GLN540	CG	THR122	OG1	3.104
GLN540	C	THR122	OG1	3.116
GLN540	NE2	THR122	OG1	3.791
GLN540	OE1	THR122	CG2	3.800
GLN540	OE1	THR122	OG1	3.488
GLN540	O	THR122	CA	3.783
GLN540	O	THR122	CB	3.338
GLN540	O	THR122	CG2	3.135
GLN540	O	THR122	OG1	2.659
ARG543	CZ	THR122	CG2	3.821
ARG543	NE	THR122	CG2	3.473
ARG543	NH2	THR122	CG2	3.402
ARG543	NH2	THR122	O	3.774

C

Mode 7: C^{α}-C^{α} distances (Å) between NCT and PS1 (closed state distances < 9 Å)

NCT	PS1	closed	open (PDB)
LEU617	THR122	6.172	25.030
THR582	PHE118	6.480	31.717
ARG583	**THR119**	**6.592**	**28.615**
THR582	ASP121	7.031	27.721
LEU617	GLU123	7.033	27.342
ASP615	**GLU123**	**7.036**	**23.747**
ARG583	PHE118	7.187	28.313
ASP541	**ARG108**	**7.266**	**25.150**
GLU584	PHE118	7.299	27.754
GLU584	**PRO117**	**7.352**	**31.037**
ASP541	LYS109	7.397	23.162
THR582	THR119	7.478	32.096
ARG616	**GLU123**	**7.559**	**24.945**
GLU584	LEU113	7.673	34.192
GLU584	TYR115	7.715	32.873
GLU584	GLN112	7.798	33.405
PRO618	THR122	7.844	23.428
GLU584	THR119	7.941	28.529
GLU584	GLY111	8.229	32.739
ARG616	THR122	8.273	22.882
GLN587	GLY111	8.333	30.926
ARG583	ASP121	8.446	24.432
ARG583	GLU120	8.462	27.851
GLU584	ILE114	8.506	34.791
ASP615	GLU120	8.632	27.906
ASN 612	TYR451	8.732	42.999
GLU613	TYR451	8.763	40.462
GLN540	LYS109	8.771	26.739
GLN587	GLN112	8.780	31.628
LEU617	ASP121	8.799	27.780
THR582	GLU120	8.799	31.222
ASP615	THR124	8.811	23.436
GLU584	THR116	8.925	32.477
PRO618	ASP121	8.975	25.836

D

Atomic interactions closer than 4 Å

ARG583	CD	THR119	OG1	3.189
ARG583	CD	THR119	O	3.644
ARG583	CZ	THR119	OG1	2.904
ARG583	NE	THR119	OG1	2.969
ARG583	NH1	THR119	OG1	3.107
ARG583	NH2	THR119	OG1	3.430
ASP615	CA	GLU123	OE2	3.733
ASP615	C	GLU123	OE2	3.603
ASP615	CB	GLU123	CG	3.980
ASP615	CB	GLU123	OE2	3.394
ASP615	CG	GLU123	OE2	3.943
ASP541	CA	ARG108	NH2	3.869
ASP541	C	ARG108	NH2	3.823
ASP541	CB	ARG108	NH2	3.461
ASP541	CG	ARG108	CZ	3.573
ASP541	CG	ARG108	NE	3.290
ASP541	CG	ARG108	NH2	2.969
ASP541	O	ARG108	NH2	3.037
ASP541	OD1	ARG108	CZ	3.334
ASP541	OD1	ARG108	NE	2.906
ASP541	OD1	ARG108	NH2	2.906
ASP541	OD2	ARG108	CB	3.932
ASP541	OD2	ARG108	CZ	3.521
ASP541	OD2	ARG108	NE	3.090
ASP541	OD2	ARG108	NH2	3.219
GLU584	CG	PRO117	O	3.777
GLU584	N	PRO117	O	3.772
ARG616	CA	GLU123	OE2	3.476
ARG616	C	GLU123	CB	3.986
ARG616	C	GLU123	CD	3.645
ARG616	C	GLU123	OE1	3.913
ARG616	C	GLU123	OE2	3.482
ARG616	N	GLU123	CD	3.611
ARG616	N	GLU123	OE2	2.667
ARG616	O	GLU123	CB	3.014
ARG616	O	GLU123	CD	3.457
ARG616	O	GLU123	CG	3.761
ARG616	O	GLU123	OE1	3.847
ARG616	O	GLU123	OE2	3.583

*(*) Cα-Cα distances refer to the closed state of the complex reached via the bending modes 1 and 7 based on an RMSD of 4 Å from the initial structure. Residue pairs coming into close proximity (< 9 Å) are listed for mode 1 (in **A**) and mode 7 (**C**). The last column in **A** and **C** lists the C_{α}-C_{α} distances in initial PDB structure. Among those residue pairs, those making atom-atom contacts within 4 Å are listed in parts **B** and **D**. See also **Figs. 5** and **S4**.*

Table S2. Summary of results from druggability simulations (*)

PS1

	run	kcal/mol
R1: Catalytic cavity		
Intact	1st	-12.21
Intact	2nd	-12.68
Intact	3rd	-12.36
PS1	1st	-13.67
PS1	2nd	-13.44
PS1	3rd	-14.36
PS1	4th	-11.57
PS1	5th	-13.63
AVG	all	-12.99 ± 1.42
R2: Allosteric site		
Intact	2nd	-11.84
Intact	3rd	-9.93
PS1	1st	-9.74
PS1	4th	-9.73
PS1	5th	-9.49
AVG	all	-10.15 ± 1.69
R3: TM2-TM6-TM9		
intact	1st	-10.01
intact	2nd	-9.90
intact	3rd	-12.29
PS1	1st	-11.32
PS1	2nd	-11.05
PS1	3rd	-11.17
PS1	4th	-10.62
PS1	5th	-10.78
AVG	all	-10.89 ± 1.40

PS1 & APH-1

	run	kcal/mol
R4: TM1-TM8 (APH-1)		
Intact	1st	-12.48
Intact	2nd	-12.82
Intact	3rd	-12.99
PS1	1st	-8.87
PS1	5th	-10.68
AVG	all	-11.57 ± 2.70
R5: TM9 top (APH-1)		
intact	1st	-9.08
intact	2nd	-9.22
PS1	4th	-9.94
AVG	all	-9.41 ± 0.53
R6: TM8-TM9 (APH-1)		
Intact	2nd	-11.76
Intact	3rd	-12.13
AVG	all	-11.95 ± 0.19

APH-1 & NCT (TM)

	run	kcal/mol
R7: APH-1, NCT-TM		
Intact	1st	-13.01
Intact	2nd	-13.44
Intact	3rd	-13.36
AVG	all	-13.27 ± 0.26

NCT

	Region	kcal/mol
NCT: Region RA to RE		
intact	RA	-10.37
Intact	RB	-9.57
intact	RC	-8.45
intact	RD	-8.17
intact	RE	-8.14

*(*) Two sets of simulations were performed: (i) a set of 5 independent runs with only PS1 (called PS1 1st – 5th), and (ii) a set of 3 independent runs for the intact protein (called intact 1st – 3rd). The druggable sites are organized by the corresponding subunits. No druggable sites were detected on PEN2. The third column in each case lists the binding free energies. Simulations yielded 6 druggable sites (R1-R6) on PS1 (**Figs. 9A-B** and **S8**) including three (R4-R6) at the interface between PS1 and APH-1; one (R7) on APH-1 at the interface with the IC terminal helix of NCT (**Fig. S8**), and five sites on the EC subunit NCT, designated as RA - RE (**Fig. 9C**).*